ARTICLE NO. 79-1501R

C80-101

Supercritical Airfoil Boundary Layer Measurements

20003
20018

F.W. Spaid*
McDonnell Douglas Corp., St. Louis, Mo.
and
L.S. Stivers Jr.†
NASA Ames Research Center, Moffett Field, Calif.

A series of experiments was conducted on flowfields about two models which had sections that were slight modifications of the original Whitcomb supercritical airfoil section. Boundary layer profiles were obtained on both upper and lower surfaces for combinations of lift coefficient and freestream Mach number, including both subcritical cases and flows with upper surface shocks. The data are intended to provide test cases for comparison with predictions of numerical computations, and to contribute to a more detailed understanding of the mechanisms associated with transonic drag rise. Comparisons are made between measured boundary layer properties and results from boundary layer computations based on measured static pressure distributions.

Nomenclature

a = function of M_e, γ, and r in van Driest transformation, Eq. (2)
c = airfoil chord
C_d = airfoil section drag coefficient
C_f = local skin friction coefficient, $C_f = \tau/q_e$
C_f^* = skin friction coefficient computed from transformed velocity profile, u^*
C_l = airfoil section lift coefficient
C_p = pressure coefficient, $C_p = (P - P_\infty)/q_\infty$
d = probe tip depth
H = boundary layer shape factor, $H = \delta^*/\theta$
M = Mach number
P = pressure
q = dynamic pressure, $q = \frac{1}{2}\rho u^2$
r = recovery factor
Re_c = Reynolds number based upon chord
u = velocity
u^* = velocity transformed by van Driest transformation, Eq. (1)
u_τ = shear velocity, $u_\tau = \sqrt{\tau_w/\rho_w}$
u^+ = transformed velocity normalized by shear velocity, $u^+ = u^*/u_\tau$
w = empirical wake function, Eq. (4)
x = coordinate measured parallel to freestream direction
z = coordinate normal to airfoil plane
z^+ = law-of-the-wall coordinate, $z^+ = (zu_\tau)/\nu_w$
α = angle of attack, deg
γ = specific heat ratio
δ = boundary layer thickness
δ^* = boundary layer displacement thickness
θ = boundary layer momentum thickness
ν = kinematic viscosity
Π = wake coefficient for transformed boundary layer profile, Eq. (3)
ρ = density
τ = shear stress

Subscripts

c = airfoil chord
e = conditions at edge of boundary layer
w = conditions at the wall (airfoil surface)
∞ = freestream conditions

Presented as Paper 79-1501 at the AIAA 12th Fluid and Plasma Dynamics Conference, Williamsburg, Va., July 23-25, 1979; submitted Aug. 8, 1979; revision received Jan. 14, 1980.

Index categories: Transonic Flow; Boundary Layers and Convective Heat Transfer—Turbulent.

*Senior Scientist, Research Laboratories. Associate Fellow AIAA.
†Aerospace Scientist, Aerodynamics Branch, now retired. Associate Fellow AIAA.

Introduction

RECENT improvements in techniques for computation of transonic flowfields about airfoils[1-4] have created a need for experimental data which can be used to evaluate the accuracy of these methods and to provide guidance for their improvements and extensions. The present study is one phase in a series of experiments on the flow about a supercritical airfoil section. The data are intended to allow comparisons with results of numerical computations in more detail than are possible when only the usual surface static pressure (lift) and far wake survey (drag) data are obtained. The experiments include significant viscous-inviscid interaction effects, but avoid situations dominated by extensive separation.

Facilities and Equipment

The experiments were part of a cooperative program between McDonnell Douglas Research Laboratories (MDRL) and the NASA Ames Research Center. They were conducted in the Two- by Two-Foot Transonic Wind Tunnel of the Ames Research Center, modified for two-dimensional research testing. Two 15.24 cm chord models of essentially the original NASA Whitcomb integral (unslotted) supercritical airfoil section were used during these experiments. One model was fabricated with a nominally sharp trailing edge, and the other had a blunt trailing edge equal to 1% chord, formed by downward rotation of the aft lower surface contour from 65% chord to the trailing edge. The test section arrangement for these experiments is shown in Fig. 1. The models spanned the test section and were installed between rotating glass windows in solid sidewalls. The top and bottom test section walls were ventilated. Boundary layer surveys were obtained with the aid of a two degree-of-freedom traversing rig and probe assembly. The height of the probe tip was 0.10 mm. More detailed information concerning the facility, the traversing rig and probe, and the blunt trailing edge model (including model coordinates) is contained in Refs. 5-7. A more detailed presentation of the present work is given in Ref. 8. Lower surface coordinates of the sharp trailing edge model are given in Table 1.

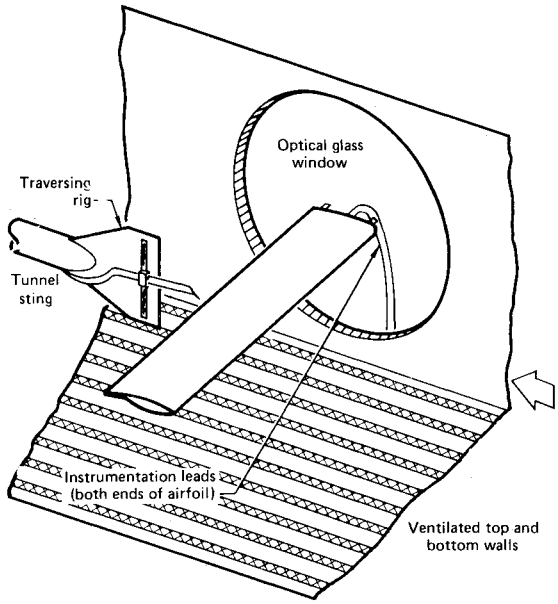

Fig. 1 Test section setup.

Results and Discussion

Surface Static Pressure Distributions

The experiments of Refs. 5-7 were conducted with leading edge boundary layer trips. If the trip is effective in causing transition to occur near the leading edge, complications associated with interaction of a shock wave with a laminar or transitional boundary layer are avoided, as are effects of interaction between an aft-located roughness strip and a turbulent boundary layer originating near a leading edge suction peak. On the other hand, locating transition strips further aft in a test at relatively low Reynolds number should result in a displacement thickness distribution near the trailing edge which would provide a better simulation of viscous-inviscid interaction effects at high Reynolds number. The recommendations of Braslow, et al.,[9] were used as guidelines in selecting trip configurations. Nominal bead diameters ranged 0.10-0.13 mm.

Static pressure distributions corresponding to cases for which boundary layer data were obtained are presented in Fig. 2. Drag data for these test conditions are presented in Ref. 8.

A comparison of static pressure data obtained with the two airfoil models at $M_\infty = 0.6$ is shown in Fig. 2e. The method of altering the coordinates from the original section shape to produce the blunt trailing edge also increased the aft camber of this model. This increased camber is at least partially responsible for the observed differences in the static pressure distributions. Some of the differences probably are caused by deviations of the actual airfoils from the theoretical coordinates.

Table 1 DSMA 523 lower-surface profile coordinates, sharp trailing edge

x/c	z/c	x/c	z/c
0.60	−0.038885	0.80	0.005224
0.62	−0.035181	0.82	0.008108
0.64	−0.030940	0.84	0.010505
0.66	−0.026087	0.86	0.012374
0.68	−0.020633	0.88	0.013645
0.70	−0.015445	0.90	0.014169
0.72	−0.010574	0.92	0.013798
0.74	−0.006027	0.94	0.012338
0.76	−0.001872	0.96	0.009726
0.78	0.001892	0.98	0.005773
		1.00	0.000498

Data obtained with the blunt trailing edge model at $M_\infty = 0.83$ are presented in Fig. 2g. Data from the present study with aft-located boundary layer trips are compared in this figure with data obtained with a leading edge trip from Ref. 5. The difference in shock location is believed to be associated with the difference in upper surface displacement thickness distribution.

Probe interference effects observed during this study are similar to, but smaller than, those reported by Cook.[10] Static pressure distributions obtained upstream of the probe location, with the probe near the surface, are superimposed in Figs. 2a and 2d on the corresponding distribution obtained with the probe retracted. Where interference effects are present, they always take the form of an additional adverse static pressure gradient superimposed on the undisturbed static pressure distribution. The magnitude of the effect decreases as the probe tip approaches the trailing edge. Probe interference effects on the static pressure distribution were always negligible (less than the run-to-run data repeatability), both at the trailing edge and slightly forward of the trailing edge on the lower surface.

Results of an attempt to determine the effects of these static pressure perturbations on boundary layer properties are summarized in Ref. 8, where it is tentatively concluded that these effects are small, if the noninterference C_p is used in computing velocities from pitot pressure data.

Boundary Layer Profile Data

A set of boundary layer data obtained with the sharp trailing edge model is presented in detail in Fig. 3. This case corresponds to $M_\infty = 0.8$, $Re_c = 3 \times 10^6$, $\alpha_{geom} = 2.4$ (Fig. 2f) and is characterized by a shock which is located relatively far aft of the trip so that effects of the trip on the shock wave/boundary layer interaction are minimized, but sufficiently far forward to permit the existence of a region of nearly constant static pressure immediately downstream of the shock, thus allowing recovery of the boundary layer profile prior to encountering the adverse pressure gradient near the trailing edge. Data reduction for the trailing edge profiles utilized information from interferograms, as described in Ref. 11.

The laminar boundary layer at $x/c = 0.3$ on the upper surface is shown in Fig. 3a. This boundary layer is approximately at the lower limit of resolution of the measuring technique. Values of overall boundary layer thickness, displacement thickness, and momentum thickness, all normalized by the chord, are tabulated and compared with values calculated by the Cebeci-Smith method.[12] Agreement between measured and computed thicknesses is good. Although no reverse flow is indicated by the lower surface boundary layer profile at $x/c = 0.91$, oil flow data obtained during a phase of this cooperative program indicate that a separation bubble was present in the lower surface concavity under these conditions. Instances where measured pitot pressures were slightly in excess of the local static pressure in regions where the flow was known to be reversed have been reported elsewhere in the literature.[13,14]

Velocity profiles corresponding to attached flow were transformed to equivalent incompressible profiles using the van Driest transformation[15]:

$$u^* = (u_e/a)\sin^{-1}[a(u/u_e)] \tag{1}$$

where

$$a = \left(\frac{r(\gamma-1/2)M_e^2}{1+r(\gamma-1/2)M_e^2}\right)^{1/2} \tag{2}$$

The subscript e refers to edge conditions and r is the recovery factor, taken to be 0.89. The transformed profiles

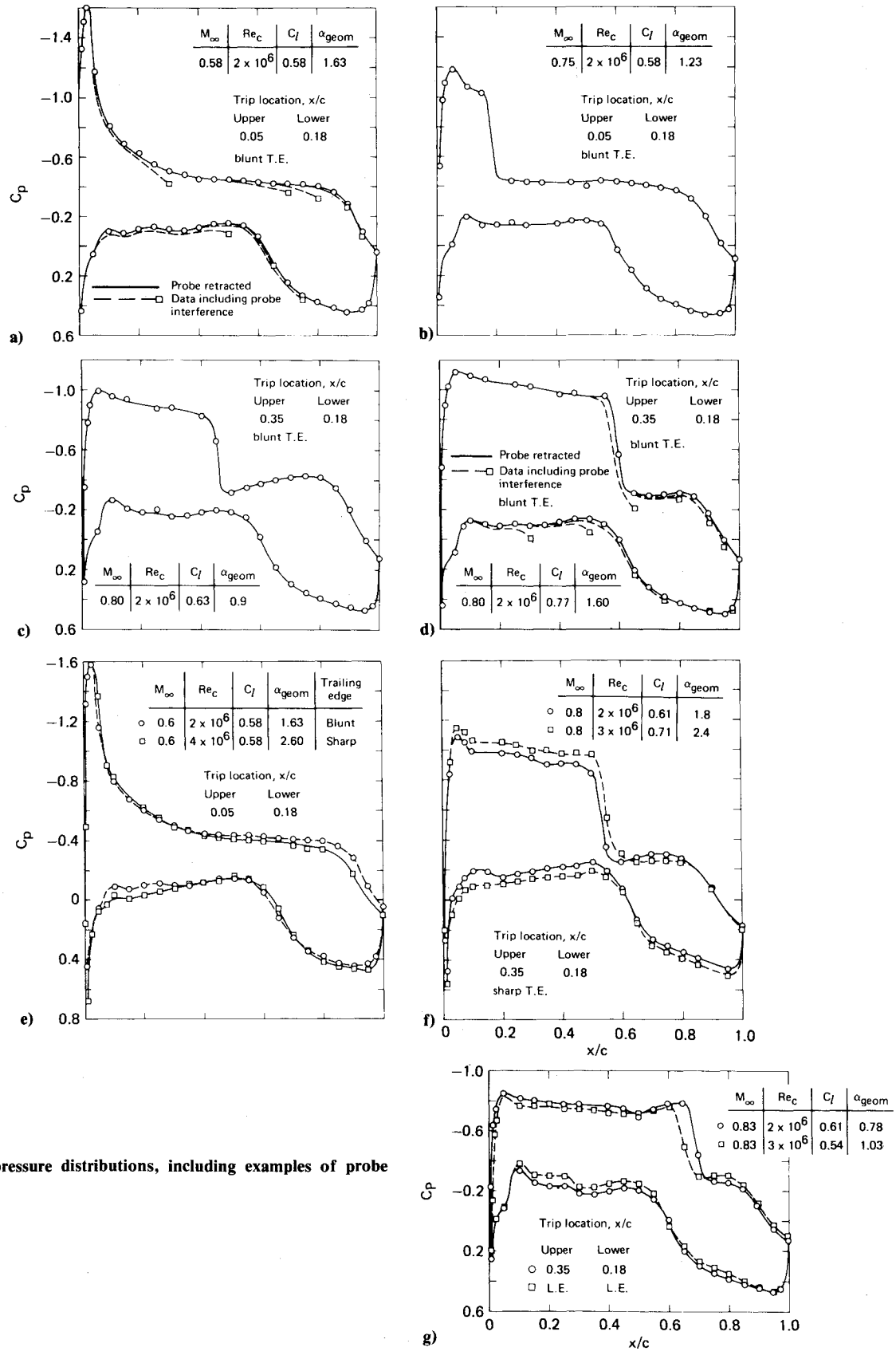

Fig. 2 Static pressure distributions, including examples of probe interference.

were fitted by an iterative least-squares technique to Coles's wall-wake formula[16]:

$$u^+ = (1/0.41)\ln z^+ + 5.0 + (\Pi/0.41)w \qquad (3)$$

$$w = 2\sin^2(\pi z/2\delta) \qquad (4)$$

The quantities u_τ, Π, and δ were determined by the fitting process. Additional details pertaining to the transformation and fitting process are given in Refs. 5 and 6. Apparently because of the abrupt expansion of the lower surface flow at the trailing edge, the lower surface trailing edge profiles did not conform to the wall-wake family, and have been excluded from this presentation. Most upper surface trailing edge

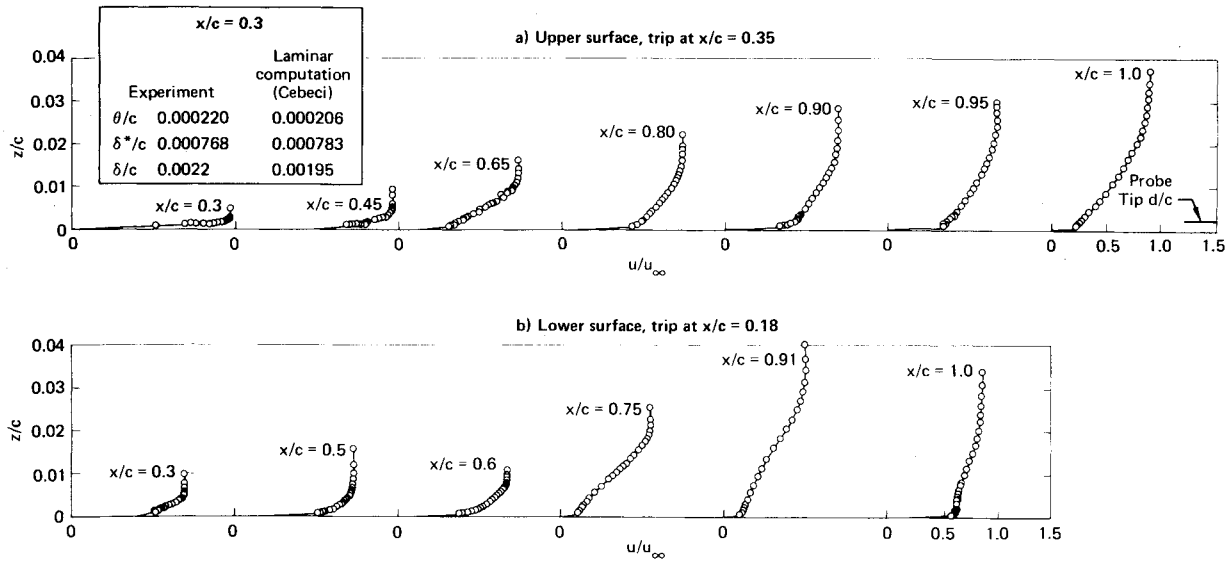

Fig. 3 Boundary layer profiles at $M_\infty = 0.8$: sharp trailing edge, $Re_c = 3 \times 10^6$, $\alpha_{geom} = 2.4$ (see Fig. 2f).

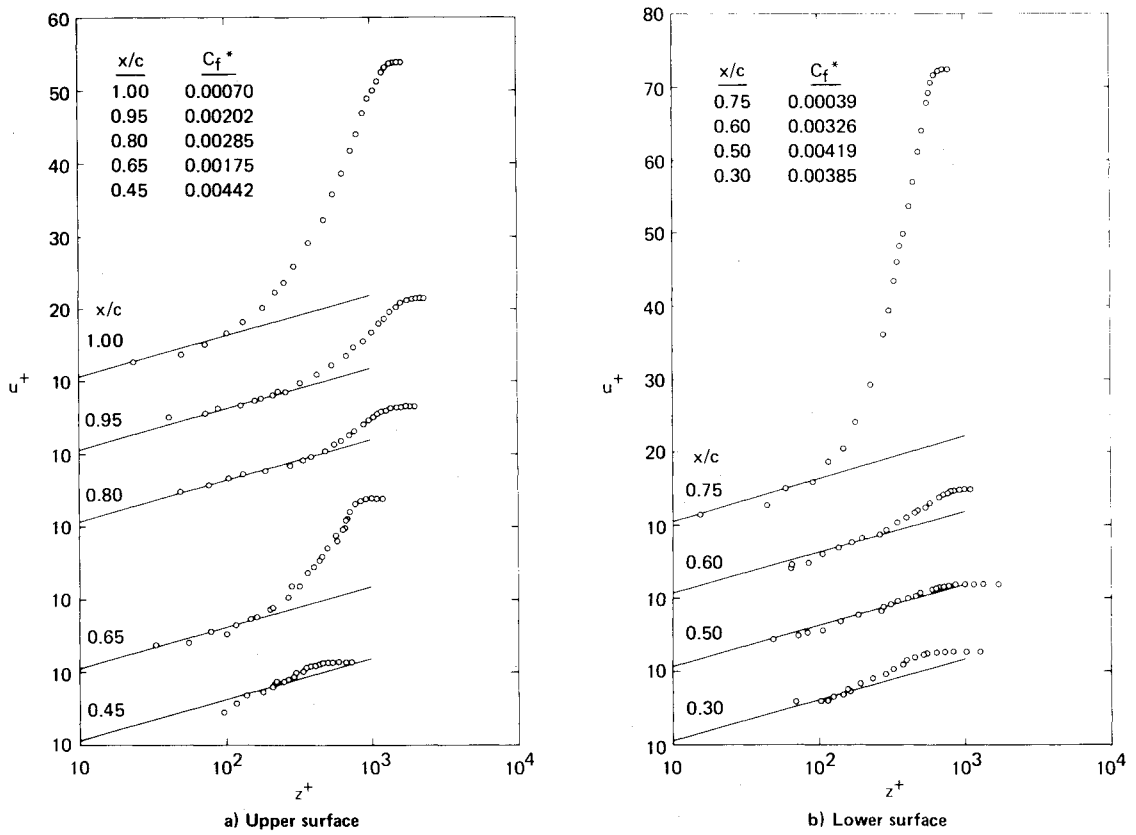

Fig. 4 Transformed boundary layer profiles in law-of-the-wall coordinates, sharp trailing edge, $M_\infty = 0.8$, $Re_c = 3 \times 10^6$, $\alpha_{geom} = 2.4$ (see Fig. 3).

profiles did not exhibit a distinct logarithmic region, implying a state of incipient separation.

The data of Fig. 3 are presented in wall-wake coordinates in Figs. 4 and 5. Some data for which the wake component of the profile was negligible have been omitted from Fig. 5.

A representative sample of the upper surface trailing edge profiles is compared with Stratford's separation profile[17] in Fig. 6.

Values of the static pressure gradient used in determining the predicted profiles of Fig. 6 were estimated from the data of Fig. 2. Figure 6a is clearly a separated profile. Since the points near the surface for Fig. 6b also lie below the predicted profile, it is probably separated too. Cases c and d are in reasonable agreement with the predicted profile, indicating a state of incipient separation. The experimental profile of Fig. 6e is probably attached, since it lies above the incipient separation profile and since a small logarithmic region exists near the surface (Fig. 4a).

Integral Properties and Comparisons with Computations

Comparisons between measured and calculated boundary layer properties are presented in Fig. 7 for the case shown in

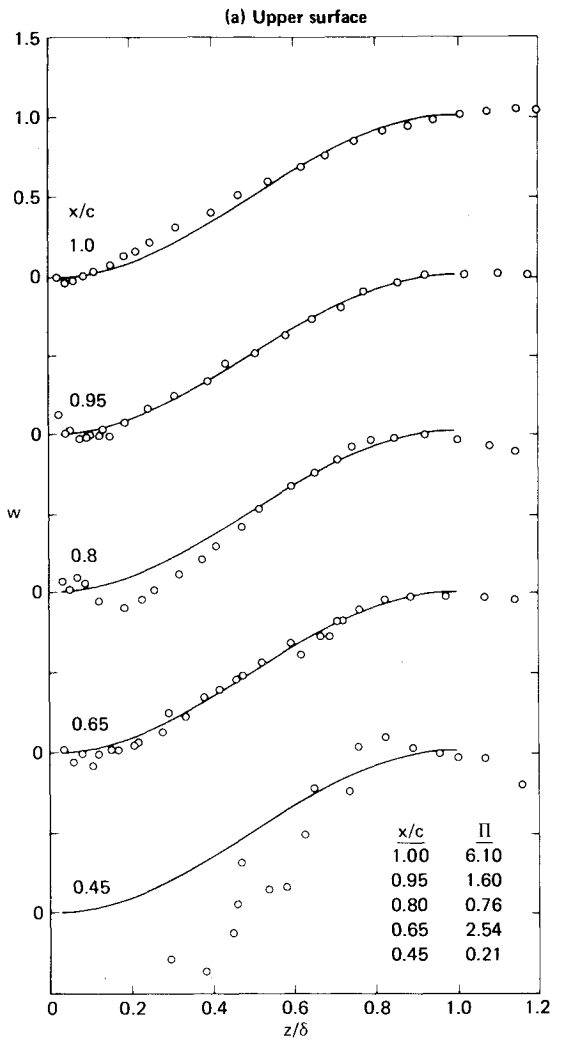

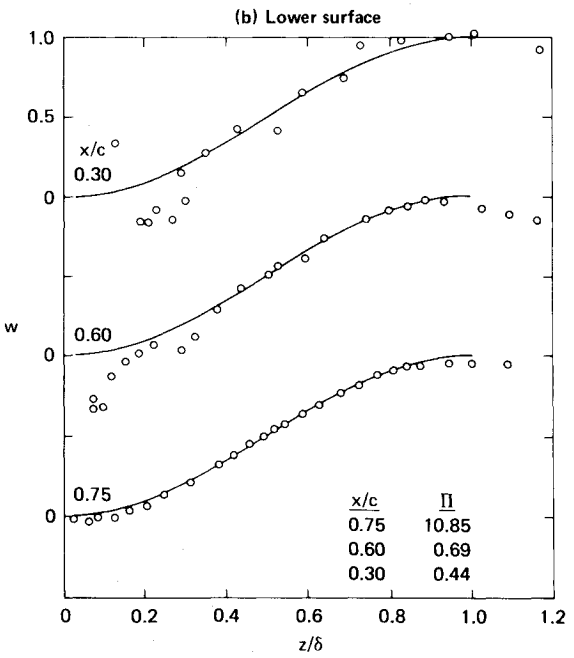

Fig. 5 Wake components of transformed boundary layer profiles, sharp trailing edge, $M_\infty = 0.8$, $Re_c = 3 \times 10^6$, $\alpha_{geom} = 2.4$ (see Fig. 3).

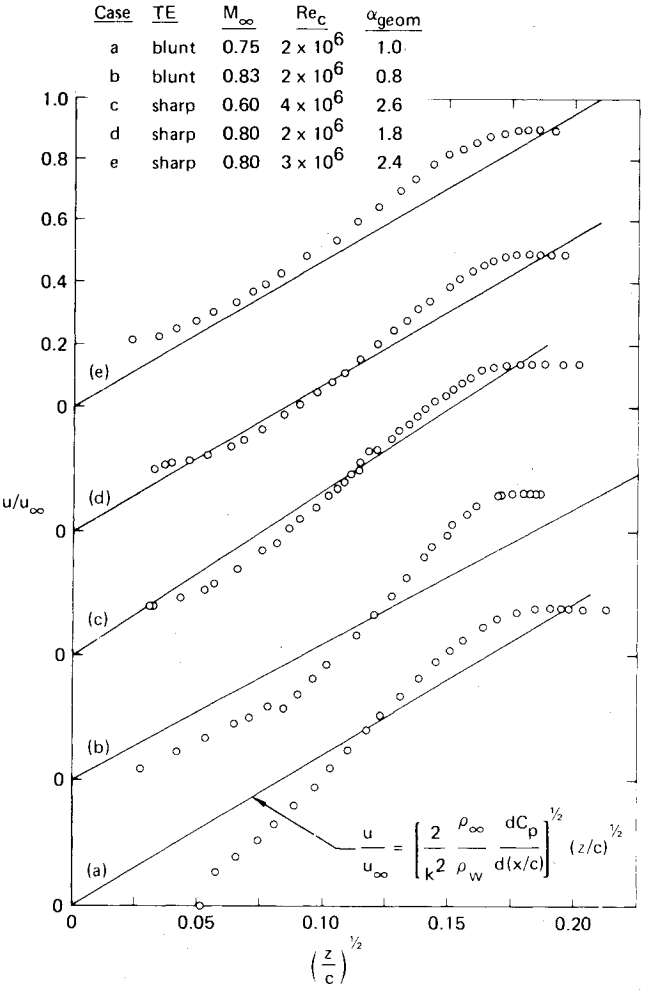

Fig. 6 Comparison of upper surface trailing edge profiles with Stratford's separation profile.

Fig. 2e, the sharp trailing edge model at $M_\infty = 0.6$. This case is probably the one for which best overall agreement would be expected between measured and calculated boundary layers. First, the flow is almost completely subcritical, so that complications caused by shock wave/boundary layer interactions are absent. Second, both the present pitot pressure measurements and oil flow results from an earlier study indicate that the flow remained attached in the lower surface concavity. Experimental momentum and displacement thicknesses for the upper surface are compared in Fig. 7a with results of computations obtained from three boundary layer computation methods, using the measured static pressure distribution. Corresponding values of skin friction are compared in Fig. 7b. The boundary layer computation methods used for this purpose are the Cebeci-Smith finite difference method[12] and two integral methods.[18,19] The Nash-Macdonald method was developed specifically for computation of boundary layers on airfoils, and has been used in combination with programs for computation of transonic airfoil flowfields.[1,4] Initial conditions for the Nash-Macdonald method for this and all subsequent cases were obtained from the Cebeci-Smith results. Agreement between measured and calculated properties is reasonably good for $x/c \leq 0.8$.

The discrepancy in C_f shown by Bower's method[18] for $0.3 < x/c < 0.4$ is caused by the use of an experimental profile for starting the calculation. The close agreement between the Cebeci-Smith computations and those of Bower's method is consistent with results from numerous similar comparisons between predictions of the Cebeci-Smith method and results

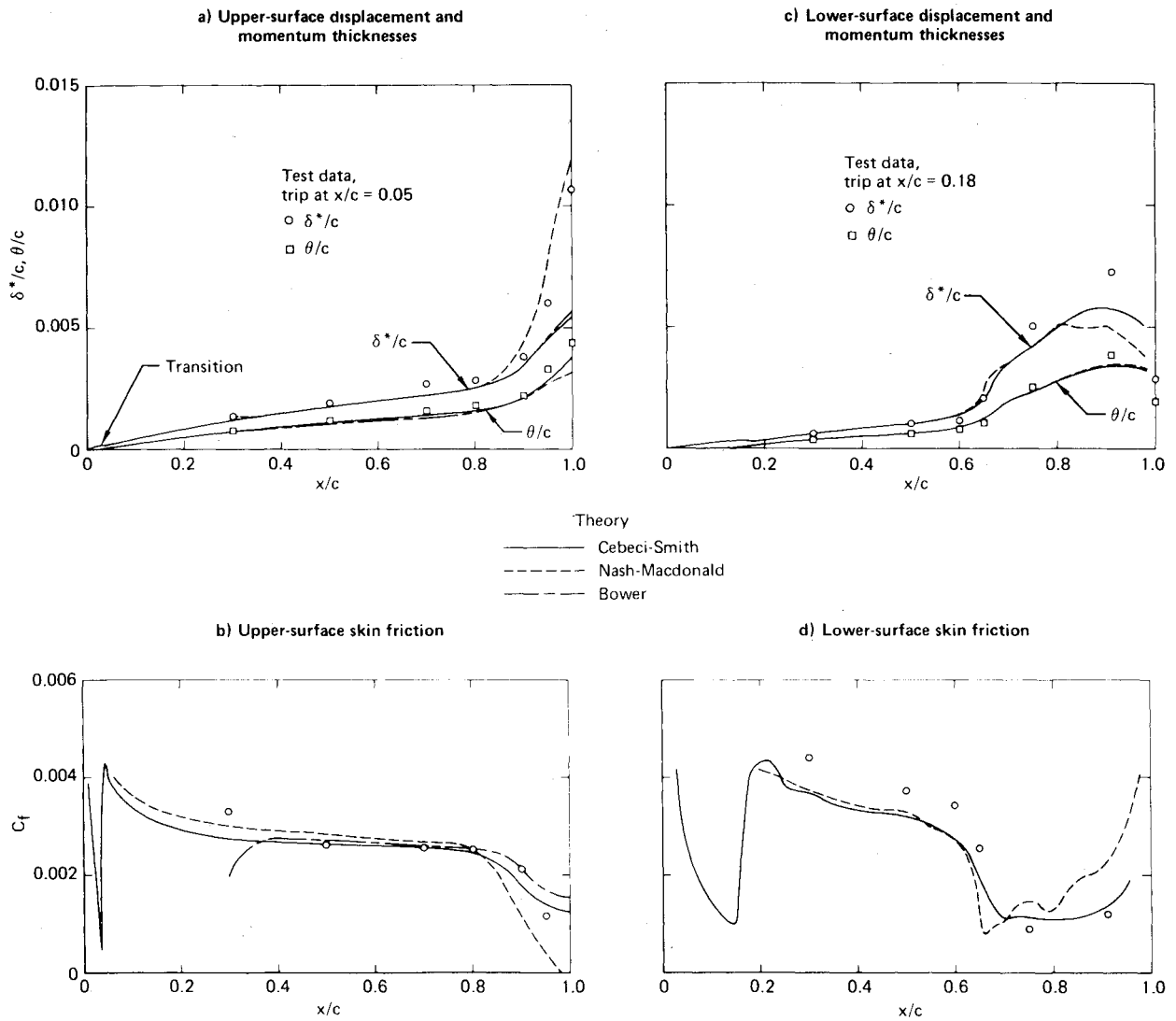

Fig. 7 Comparison between measured and calculated boundary layer properties: sharp trailing edge, $M_\infty = 0.6$, $Re_c = 4 \times 10^6$, $\alpha_{geom} = 2.6$ (see Fig. 2e).

from the methods of Reeves[20] and Bradshaw.[21] Near the trailing edge, the Nash-Macdonald predictions depart drastically from those of the other schemes; the computed displacement thicknesses exceed measured values. Since the computed momentum thickness is underpredicted, this situation corresponds to a computed shape factor distribution that is much larger than the experimental distribution. Separation just upstream of the trailing edge is indicated by the computed skin friction distribution.

The Nash-Macdonald method contains a direct dependence of a boundary layer shape factor parameter on the local static pressure gradient which was derived from a correlation of airfoil boundary layer data restricted to adverse pressure gradients. Apparently this correlation causes the resulting prediction of displacement thickness development near the trailing edge to differ from that of the other methods, and to agree better with the experimental data in this region. Since the boundary layer formulation is invalid in the immediate vicinity of the trailing edge, this agreement is partially fortuitous.

A similar set of comparisons for the lower surface is presented in Figs. 7c and 7d. Agreement between both sets of calculations and the data is reasonably good upstream of the concavity. Both methods underpredict the growth of displacement thickness. The skin friction predictions of Cebeci and Smith are in better agreement with the experimental data.

Comparisons involving both upper and lower surfaces are shown in Fig. 8 for the case of the blunt trailing edge model at $M_\infty = 0.75$.

In this case, and in all subsequent cases involving shock wave/boundary layer interaction, care was taken in the definition of the static pressure distribution which was used for boundary layer calculations. In a study reported by Lynch,[22] boundary layer properties computed by the Cebeci-Smith method downstream of a shock-induced pressure rise showed sensitivity to the extent of streamwise smoothing of the static pressure distribution. The calculations presented here utilized static pressure distributions in which the shock-induced pressure rise was smoothed over a streamwise distance of 8-10 times the upstream value of δ, which was the most abrupt pressure rise that could be treated by the Cebeci-Smith program for the present sets of experimental data. Examination of a summary of experimental shock wave/boundary layer interaction data presented by Inger[23] indicates that this degree of smoothing of the wall static pressure distribution is of the correct order of magnitude.

The data of Fig. 8 were obtained from two tests involving separate model installations. These results indicate that data repeatability was reasonably good; the most important source of discrepancies is probably associated with unavoidable differences in the boundary layer transition strips. Both the Cebeci-Smith and the Nash-Macdonald methods are in good agreement with the measurements downstream of the shock.

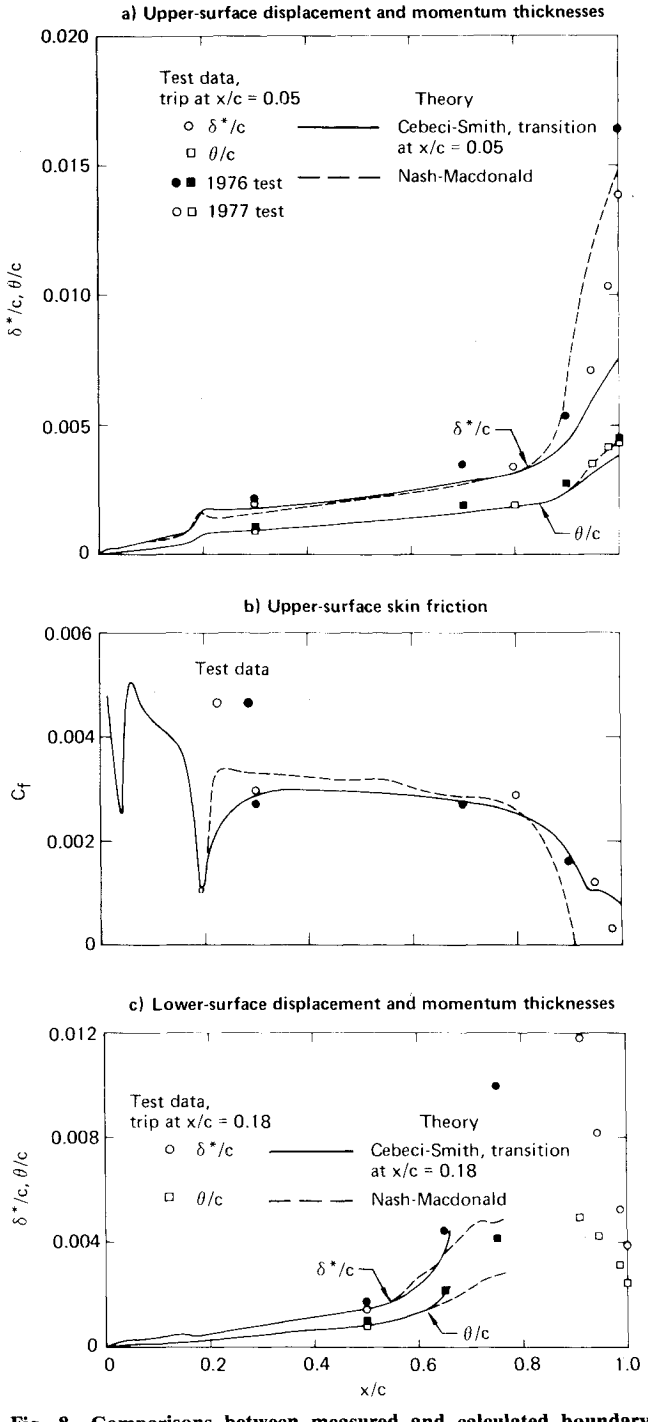

Fig. 8 Comparisons between measured and calculated boundary layer properties: blunt trailing edge, $M_\infty = 0.75$, $Re_c = 2 \times 10^6$, $\alpha_{geom} = 1.23$ (see Fig. 2b).

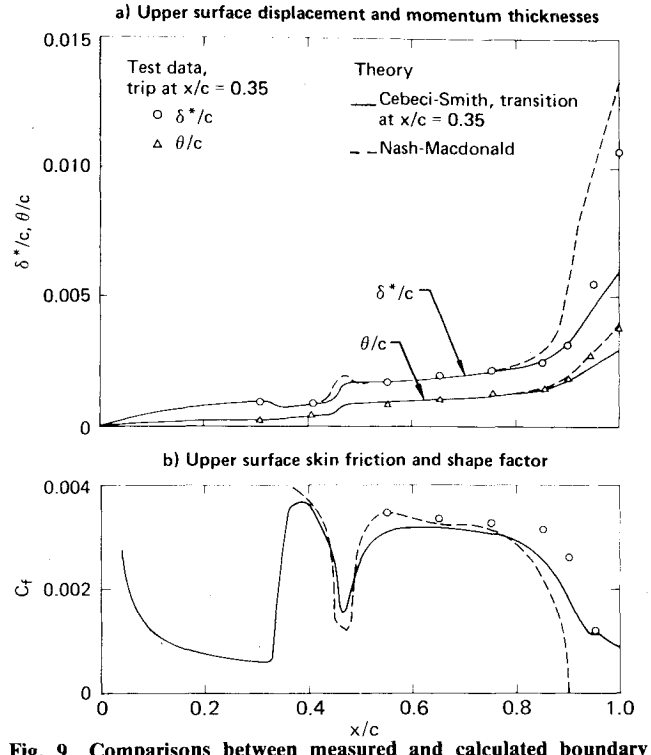

Fig. 9 Comparisons between measured and calculated boundary layer properties: blunt trailing edge, $M_\infty = 0.8$, $Re_c = 2 \times 10^6$, $\alpha_{geom} = 0.9$ (see Fig. 2c).

Note that the Nash-Macdonald skin friction decreased to zero at $x/c = 0.91$. Downstream of this point, the calculation proceeds using a constant value of shape factor parameter which has little physical significance.

The comparisons of Fig. 8c, involving lower surface momentum and displacement thicknesses, are typical of the remaining lower surface results. The large experimental values of shape factor δ^*/θ in the lower surface concavity indicate that the flow was separated, even though the measured pitot pressures were always greater than the static pressure. In this case, the Cebeci-Smith and the Nash-Macdonald predictions are in good agreement with the data at the first two stations, but the Cebeci-Smith predictions indicate separation at the third station probably not far from the actual separation point. The Nash-Macdonald method predicted attached flow for this later station, as well as for all of the remaining lower surface flows. Since neither formulation is valid for flow at or downstream of separation, comparisons downstream of a physical separation location are not meaningful.

Results obtained with the blunt trailing edge nearer the design condition, $M_\infty = 0.8$, are shown in Fig. 9. In this case, and in all of the following cases, the upper surface boundary layer trip was located at $x/c = 0.35$. Good agreement between measured and computed values of both momentum and displacement thicknesses is shown for the laminar boundary layer upstream of the trip. Agreement of all calculated quantities with experiment from $0.5 \leq x/c \leq 0.85$ is good, a result not anticipated since none of the details of the shock wave/boundary layer interactions are considered.

The sensitivity of the Nash-Macdonald method to local static pressure gradients is manifested in a peak in the displacement thickness at the shock. Neither method is accurate near the trailing edge, where the Nash-Macdonald method again predicts early separation, based upon computed C_f.

Three sets of upper surface data are presented in Fig. 10 for both blunt and sharp trailing edge models at $M_\infty = 0.80$, and the blunt trailing edge model at $M_\infty = 0.83$. Agreement between measured and calculated boundary layers on the forward portion of the airfoil is reasonably good. These cases correspond to stronger, more aft-located shock waves on the upper surface than those shown in Fig. 9, and the increases in boundary layer thicknesses caused by the interactions are correspondingly greater. Predictions of these increases are also good.

The Cebeci-Smith predictions of displacement and momentum thickness fail at $0.90 < x/c < 0.95$. Further study is needed to determine whether the boundary layer calculations are accurate throughout the entire region where the formulation is valid, since if a special treatment of the trailing edge region is employed, such as that proposed by Melnik, et al.,[3] the upstream boundary conditions provided by the conventional calculation must be accurate.

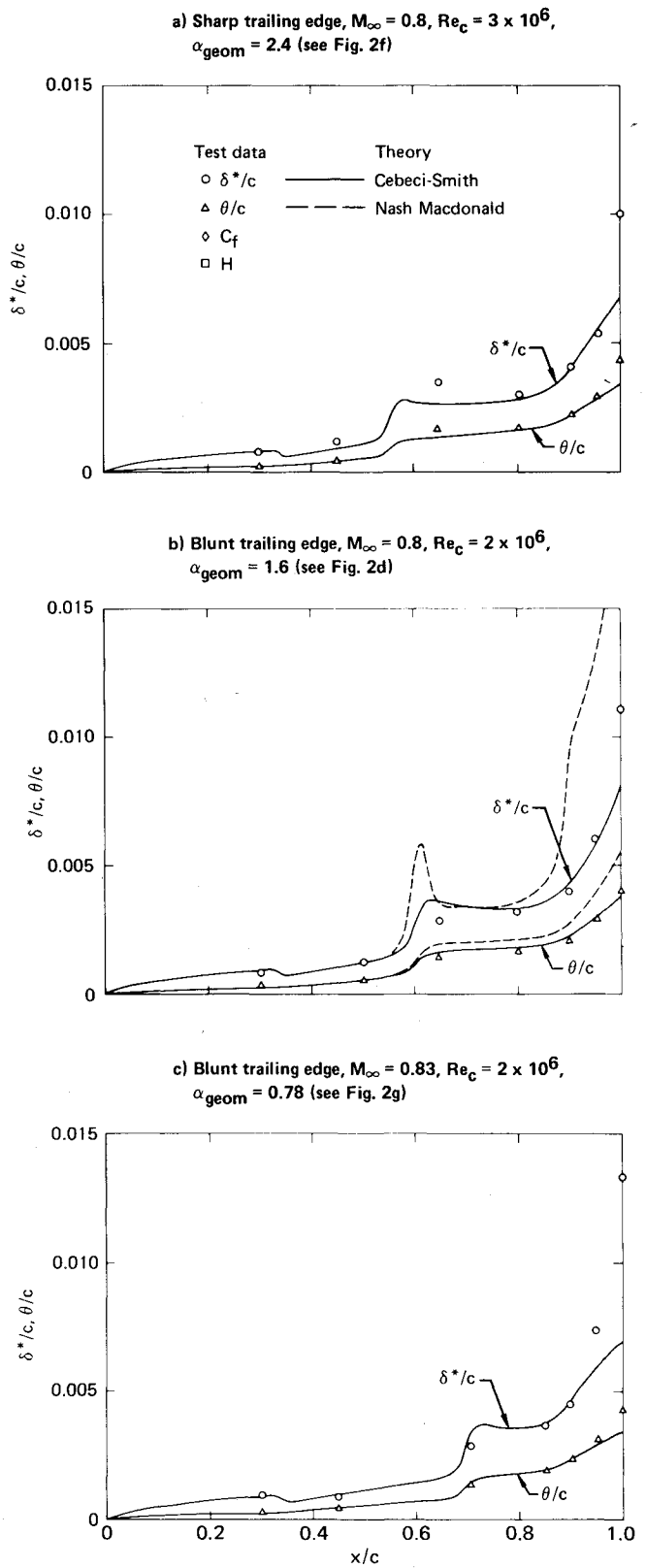

Fig. 10 Comparisons between measured and calculated upper surface boundary layer properties: boundary layer trip at $x/c = 0.35$, shocks aft of $x/c = 0.5$.

A typical example of a Nash-Macdonald prediction for this type of case is included in Fig. 10b, where a large overshoot in displacement thickness occurs at the shock, and the predicted displacement thicknesses near the trailing edge are too large.

The data of Fig. 10c correspond to the case described in detail in Refs. 5 and 6, except for the previously mentioned difference in boundary layer trip location (see Fig. 2g). The present data show the expected thinner boundary layer over the aft portion of the airfoil, associated with aft movement of transition, and also better agreement between measured and computed increases in momentum and displacement thicknesses caused by the shock.

Conclusion

Several sets of boundary layer data were obtained on both the upper and lower surfaces of a supercritical airfoil section for both predominately subcritical flows and flows with upper surface shock waves. For cases characterized by upper surface shock waves near midchord, upper surface boundary layer transition was fixed at 35% chord in order to achieve near the trailing edge a boundary layer thickness distribution representative of a Reynolds number range higher than that at which the experiments were conducted. Attached profiles, transformed by the van Driest transformation, are in good agreement with Coles' profile family.

Comparisons made between measured boundary layer properties and results from boundary layer computations show the following features:

1) The upper surface predictions of the Cebeci-Smith method are reasonably good, except near the trailing edge where the discrepancies are at least partially a result of the breakdown of the boundary layer approximations. The generally good agreement between theory and experiment downstream of the shock wave/boundary layer interactions supports the suggestion of Melnik, et al.,[3] that special treatment of such interactions may not be necessary for engineering calculations when the flow remains attached.

2) The Nash-Macdonald method predicts thicker boundary layers near the trailing edge, but the predicted displacement thicknesses are often considerably greater than the measured values. The sensitivity of this method of the local pressure gradient produces peaks in the displacement thickness distributions at the shock.

Both methods give fairly accurate results on the lower surface when the flow remains attached.

Acknowledgment

This research was conducted under the McDonnell Douglas Independent Research and Development Program in cooperation with the NASA Ames Research Center.

References

[1] Garabedian, P.R., "Computational Transonics," *Aerodynamic Analyses Requiring Advanced Computers*, NASA SP-347, Part II, Paper 44, 1975, pp. 1269-1280.

[2] Deiwert, G.S., "Numerical Simulation of High Reynolds Number Transonic Flows," *AIAA Journal*, Vol. 13, Oct. 1975, pp. 1354-1359.

[3] Melnik, R.E., Chow, R., and Mead, H.R., "Theory of Viscous Transonic Flow Over Airfoils at High Reynolds Number," AIAA Paper 77-680, 10th Fluid and Plasmadynamics Conference, Albuquerque, New Mex., June 27-29, 1977.

[4] Carlson, L.A. and Rocholl, B.M., "Application of Direct-Inverse Techniques to Airfoil Analysis and Design," *Advanced Technology Airfoil Research*, NASA C.P. 2045, Vol. 1, 1978, pp. 55-72.

[5] Hurley, F.X., Spaid, F.W., Roos, F.W., Stivers, L.S., Jr., and Bandettini, A., "Detailed Transonic Flow Field Measurements about a Supercritical Airfoil Section," NASA TM X-3244, July 1975.

[6] Hurley, F.X., Spaid, F.W., Roos, F.W., Stivers, L.S., Jr., and Bandettini, A., "Supercritical Airfoil Flowfield Measurements," *Journal of Aircraft*, Vol. 12, Sept. 1975, pp. 737-744.

[7] Spaid, F.W., Hurley, F.X., and Hellman, T.H., "Miniature Probe for Transonic Flow Direction Measurements," *AIAA Journal*, Vol. 13, Feb. 1975, pp. 253-255.

[8] Spaid, F.W. and Stivers, L.S., Jr., "Supercritical Airfoil Boundary-Layer Measurements," AIAA Paper 79-1501, 12th Fluid and Plasmadynamics Conference, Williamsburg, Va., July 23-25, 1979.

[9] Braslow, A.L., Hicks, R.M., and Harris, R.V., Jr., "Use of Grit-Type Boundary-Layer-Transition Trips on Wind-Tunnel Models," NASA TN D-3579, Sept. 1966.

[10] Cook, T.A., "Measurements of the Boundary Layer and Wake of Two Aerofoil Sections at High Reynolds Numbers and High-Subsonic Mach Numbers," (British) R.&M. 3722, 1973.

[11] Spaid, F.W. and Bachalo, W.D., "Experiments on the Flow About a Supercritical Airfoil, Including Holographic Interferometry," AIAA Paper 80-0343, 18th Aerospace Sciences Meeting, Pasadena, Calif., Jan. 14-16, 1980.

[12] Cebeci, T. and Smith, A.M.O., *Analysis of Turbulent Boundary Layers*, Academic Press, New York, 1974, pp. 258-384.

[13] Vidal, R.J., Wittliff, C.E., Catlin, P.A., and Sheen, B.H., "Reynolds Number Effects on the Shock Wave-Turbulent Boundary-Layer Interaction at Transonic Speeds," AIAA Paper 73-661, 6th Fluid and Plasmadynamics Conference, Palm Springs, Calif., July 16-18, 1973.

[14] Kooi, J.W., "Experiment on Transonic Shock-Wave Boundary Layer Interaction," *Flow Separation*, AGARD CP-168, Nov. 1975.

[15] van Driest, E.R., "Turbulent Boundary Layer in Compressible Fluids," *Journal of the Aeronautical Sciences*, Vol. 18, March 1951, pp. 145-160.

[16] Coles, D.E., "The Young Person's Guide to the Data," *Proceedings: Computation of Turbulent Boundary Layers*, 1968 AFOSR-IFP-Stanford Conference, Vol. II, Compiled Data, D.E. Coles and E.A. Hirst, Eds., Stanford University, 1969.

[17] Stratford, B.S., "The Prediction of Separation of the Turbulent Boundary Layer, *Journal of Fluid Mechanics*, Vol. 5, Part 1, Jan. 1959, pp. 1-16.

[18] Bower, W.W., "Analytical Procedure for the Calculation of Attached and Separated Subsonic Diffuser Flows," *Journal of Aircraft*, Vol. 13, Jan. 1976, pp. 49-56.

[19] Nash, J.F. and Macdonald, A.G.J., "The Calculation of Momentum Thickness in a Turbulent Boundary Layer at Mach Numbers up to Unity," British Aeronautical Research Council C.P. 963, 1967.

[20] Reeves, B.L., "Two-Layer Model of Turbulent Boundary Layers," *AIAA Journal*, Vol. 12, July 1974, pp. 932-939.

[21] Bradshaw, P. and Unsworth, K., "An Improved FORTRAN Program for the Bradshaw-Ferriss-Atwell Method of Calculating Turbulent Shear Layers," Imperial College of Science and Technology, Aero Report 74-02, 1974.

[22] Lynch, F.T., "Recent Applications of Advanced Computational Methods in the Aerodynamic Design of Transport Aircraft Configurations," Douglas Paper 6639, 11th Congress of ICAS, 1978.

[23] Inger, G.R., "Analysis of Transonic Normal Shock-Boundary Layer Interaction and Comparisons with Experiment," AIAA Paper 76-331, 9th Fluid and Plasmadynamics Conference, San Diego, Calif., July 1976.